OPEN ACCESS

Use of Multielectrode Arrays and Statistical Analysis to Investigate the Pitting Probability of Copper. Part I: The Effect of Chloride

Journal of The Electrochemical Society, 2022 **169** 061503

Use of Multielectrode Arrays and Statistical Analysis to Investigate the Pitting Probability of Copper. Part I: The Effect of Chloride

Sina Matin,[1] Arezoo Tahmasebi,[2] Mojtaba Momeni,[1] Mehran Behazin,[3] Matt Davison,[2] David W. Shoesmith,[1,4] and James J. Noël[1,4,*,z]

[1]*Department of Chemistry, Western University, London, ON, N6A 5B7, Canada*
[2]*Department of Statistical and Actuarial Sciences, Western University, London, ON, N6A 5B7, Canada*
[3]*Nuclear Waste Management Organization, Toronto, ON, M4T 2S3, Canada*
[4]*Surface Science Western, Western University, London, ON, N6G 0J3, Canada*

Under some conditions, copper and copper alloys are either immune from corrosion or undergo slow uniform corrosion, generally considered a favourable situation, since predicting the damage incurred by the metal during a period of uniform corrosion is relatively straightforward. However, under conditions leading to surface passivation of Cu, localized corrosion might occur in the presence of aggressive oxidants. Therefore, the susceptibility of Cu to localized corrosion must be considered carefully to avoid unpredictable failures in Cu-based structures. Understanding the pitting probability of Cu is important for various applications, including the use of Cu-coated containers for the permanent disposal of used nuclear fuel. In this study, the pitting probability of Cu in chloride-containing solutions crudely representing the groundwater that might be found in a deep geologic repository (DGR) was investigated using electrochemical techniques and statistical analysis. The probabilities of both pitting and repassivation of Cu were found to increase with increasing [Cl^-]. The surface morphologies of copper electrodes in the same solution were also evaluated using scanning electron microscopy (SEM). The passive film on the surface of the copper electrode with the highest breakdown potential (E_b) was found to be more protective than that on the electrode with the lowest E_b.
 [DOI: 10.1149/1945-7111/ac78d3]

Manuscript submitted February 20, 2022; revised manuscript received May 2, 2022. Published June 27, 2022.

Corrosion scientists have primarily focused on the deterministic behaviour of corrosion parameters. Macdonald and coworkers investigated the deterministic behaviour of corrosion processes on a wide variety of materials, including copper, nickel, aluminum, carbon steel, manganese steel, and Fe-17Cr.[1–5] They modified damage function analysis (DFA) by making a connection between DFA and statistical methods such as extreme value statistics, unifying the deterministic and statistical approaches for predicting localized corrosion.[5] Although the detailed corrosion mechanisms surely differ between the various materials and classes of materials, yet the concepts of determinism and statistical distributions of parameters can be considered universally.

MacDonald and coworkers proposed that the pitting potential is distributed normally when the diffusivity of the cation vacancy in the oxide follows a log-normal distribution.[3,4] Moreover, a Monte-Carlo model was used to develop a deterministic model for evaluating the delayed repassivation rate constant of stable pits, with a focus on carbon steel.[1] However, due to the stochastic nature of localized corrosion, a statistical approach can be extremely powerful in providing additional insight into the possibility of localized corrosion processes occurring, and their distribution. Statistics is one of the most important tools in materials science and engineering since we work with extreme values in order to investigate the time to failure of materials, looking for the rare events that yield early and perhaps unexpected failures.

Some researchers have used extreme-value statistics to evaluate the maximum pit depth[6,7] on aluminum and wrought iron. Shibata[8] proposed that the scattering of pitting corrosion data on carbon steels and stainless steels was because of the intrinsic nature of the pitting process rather than due to uncontrolled parameters. However, the validity of this proposal remains in question, since we have control of only a few parameters such as solution condition, and not of all parameters such as the precise surface condition of all parts of each electrode (e.g., the grain orientations). Therefore, the dispersion of pitting corrosion data may result from differences in these uncontrolled experimental parameters.

Pitting corrosion of copper has been proposed to be a deterministic process and to only occur when the potential of the Cu was raised above 375 mV vs SHE in Brussels water.[9] However, this hypothesis was rejected by Shalaby[10] who claimed that the pitting potential of Cu is not a deterministic value but rather a distributed value that depends on different factors such as scan rate, solution composition, pH, and the chemical composition of Cu.

Whether certain corrosion parameters are deterministic or distributed has been an ongoing debate between corrosion researchers for many years. For instance, the critical pitting temperature (CPT) for various types of stainless steel was determined and assumed to be a singular deterministic value;[11–13] however, Frankel and coworkers[14] determined that the CPT is a distributed value, not a deterministic value. Their research clarified that the distribution range of the CPT in 316 L stainless steel is inversely proportional to the concentration of aggressive anions. Additionally, many metastable pitting events were observed at temperatures above the CPT, confirming that the CPT is neither deterministic nor an intrinsic material property. However, no researchers have yet observed a CPT in Cu materials.

Williams[15–17] introduced a stochastic pitting model that can be used to evaluate the effect of passive film breakdown on the pitting probability of stainless steel, which might also be useful for other materials such as Cu. He observed that the frequency of micropits decreased with increasing passive film thickness, specifically when the concentrations of aggressive anions were low, resulting in higher pitting potentials and a larger dispersion of values.

Provided that passive conditions can be achieved, the susceptibility to pitting is commonly evaluated by a comparison of the corrosion potential (E_{corr}), measured under open circuit conditions, to the passive film breakdown potential (E_b) measured in a potentiodynamic scan of the applied potential (E) from low to high values. Spontaneous pitting of Cu is taken to be possible if $E_{corr} \geqslant E_b$.[18,19] However, both E_{corr} and E_b are distributed parameters, due to the stochastic nature of passive film breakdown, making the boundary between non-susceptibility and susceptibility uncertain. A more conservative evaluation of susceptibility involves the evaluation of the difference between E_{corr} and the repassivation potential (E_{rp}), with the latter recorded by scanning E from above E_b, on an electrode undergoing pitting corrosion, to a value below E_b at which

*Electrochemical Society Member.
[z]E-mail: jjnoel@uwo.ca

the measured current achieves the low value measured in the passive region. E_{rp} is commonly referred to as the critical pitting potential.[19]

A number of studies have been conducted to determine the influence of various parameters relevant to DGR conditions on E_{corr}, E_b and E_{rp} of Cu.[19–23] Based on these studies, three different regions of behaviour have been claimed for Cu, based on pH:[19] uniform corrosion at pH < 7; a pitting susceptibility region between pH 7 and pH 10; and limited susceptibility at pH > 10. However, these boundaries were found to be dependent on anion type and concentration, temperature, and $[O_2]$ (when experiments were conducted under open circuit conditions). In general terms, an increase in temperature was observed to promote active behaviour of Cu, although it has been claimed that passivity is enhanced by an increase in temperature (E_b increased) possibly due to an improvement in film properties.[24] Values of E_{rp} were found to be very dependent on the relative concentrations of various anions (Cl^-, SO_4^{2-}, HCO_3^-/CO_3^{2-}, OH^-), with Cl^- generally destabilizing passive oxide films, eventually leading to active behaviour, while HCO_3^-/CO_3^{2-} enhanced passivity, and the influence of SO_4^{2-} was ambiguous but with a tendency to promote pitting. Since Cl^- levels in a Canadian DGR are anticipated to be between 1 and 5 M,[25,26] an understanding of the corrosion process in Cl^--containing solutions and the impact of Cl^- on the properties of the oxide film on Cu are essential.

The boundary between active and passive behaviour as a function of pH and $[Cl^-]$ was defined approximately by Qin et al.[23] This boundary was developed based on only a small number of experiments and does not account for the statistical distributions of the parameters measured to establish it. In the current study, a Cu multielectrode array was used to produce the distributions of values in the passive region by measuring E_{corr}, E_b and E_{rp} on 30 electrodes simultaneously.

Experimental Methodology

Copper specimens were fabricated from O-free, P-doped wrought Cu supplied by the Swedish Nuclear Fuel and Waste Management Company (SKB, Solna, Sweden). Electrodes were machined in the form of bullet specimens (18 mm height × 5 mm diameter) with one rounded end (Fig. 1) to avoid edge effects during electrochemical experiments, with a threaded connection to a stainless steel rod to enable connection to external electrochemical equipment. Specimens used in corrosion experiments were ground with a sequence of SiC papers with grit sizes of 600, 800, 1200, 2500, and 4000. The grinding was followed by rinsing in Type I water with a resistivity of 18.2 MΩ·cm (produced by a Thermo Scientific Barnstead Nanopure 7143 ultra-pure water system), sonication in ethanol to remove any grinding residues and organic contaminants, and finally drying in a stream of Ar gas.

Solution preparation.—Solutions were prepared with reagent-grade sodium chloride (NaCl, 99.0%), purchased from Fisher Scientific, and Type I water. The multielectrode array was exposed to solutions containing various concentrations of chloride in the range from 0.01 M to 1 M. The pH of the solutions was adjusted to 11 by adding small volumes of NaOH solution. It should be noted that the pH of the solutions was deliberately adjusted to a much higher value than expected in a Canadian DGR such that passivity and subsequently pitting became possible, thereby enabling an investigation of the phenomenon. As such, this work investigates an approach and methodology, but does not address the likelihood of pitting corrosion on Cu-coated containers for used nuclear fuel under anticipated DGR conditions, which is expected to be much lower than in the studies reported here.

Electrochemical cell, instrumentation, and procedure.—All potentiodynamic experiments were performed in an electrochemical cell consisting of a glass vessel containing a saturated calomel reference electrode (SCE, 0.242 V vs SHE (standard hydrogen electrode)), a Pt plate as the counter electrode, and 30 Cu specimens, each with an exposure area of 1 cm^2, as working electrodes, with a spacing of 3 cm between each electrode. The counter electrode had a large surface area and was not a limiting factor in the current measurements.

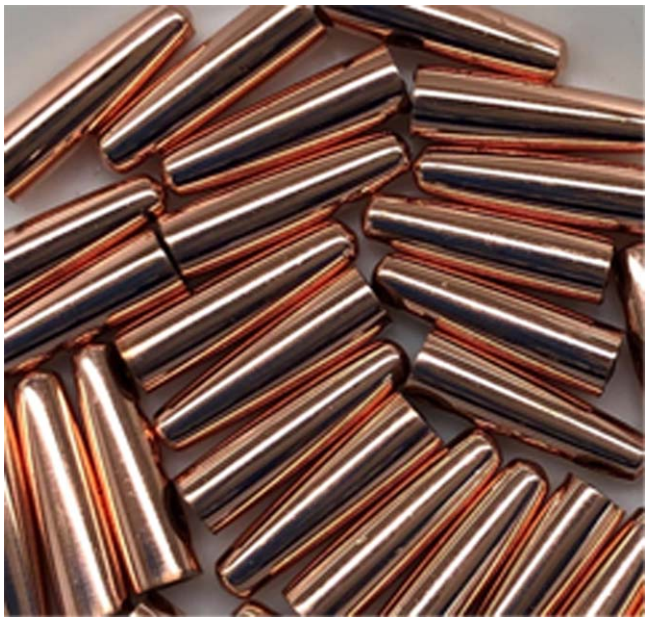

Figure 1. O-free, P-doped copper electrodes.

The electrochemical cell was placed inside a Faraday cage to reduce electrical noise from external sources. E_{corr} measurements were collected and potentiodynamic polarization experiments were conducted at a scan rate of 10 mV min^{-1} using a Multichannel Microelectrode Analyzer 910 (MMA, Scribner Associates) connected to a computer equipped with MMAlive software. The instrument was equipped with 100 μA zero-resistance ammeters (ZRA) to measure the current flow to or from each electrode individually and electrometers to measure the potential of each electrode. Figure 2 shows a schematic illustration of the experimental arrangement and photographs of the setup and array configuration. The E_b and E_{rp} values were measured in separate experiments to ensure that E_{rp} measurements were made on electrodes that were treated as identically as possible to eliminate some controllable sources of variations in this parameter. Typically, repassivation is measured on the return sweep of a scan used to determine the breakdown potential, but we have adopted a procedure (described below) to ensure that all 30 Cu specimens had experienced passive film breakdown for the same amount of time before repassivation. Experiments under each set of conditions were conducted two times each, such that data were collected from 60 electrodes in total under each set of test conditions.

Breakdown potential (E_b) measurements.—Values of E_b were measured using potentiodynamic scans in solutions containing different concentrations of $[Cl^-]$. Prior to each scan, Cu electrodes were cathodically treated at −0.85 V vs SCE for 3 min, a procedure known to help improve the reproducibility of many electrochemical experiments. The potential of −0.85 V vs SCE was selected because it was low enough to generate a small cathodic current (which may contribute to some oxide reduction and the desorption of organic contaminants from the electrode surface), but still above the potential (∼−0.95 V vs SCE) at which we have observed hydrogen absorption into Cu metal, which we do not want to occur. Then, E_{corr} was monitored for 30 min to allow a steady state to be established and to determine the range of E_{corr} values using the multielectrode array. The potential was then scanned in the positive direction from E_{corr} at a scan rate of 10 mV min^{-1} until the current on all electrodes

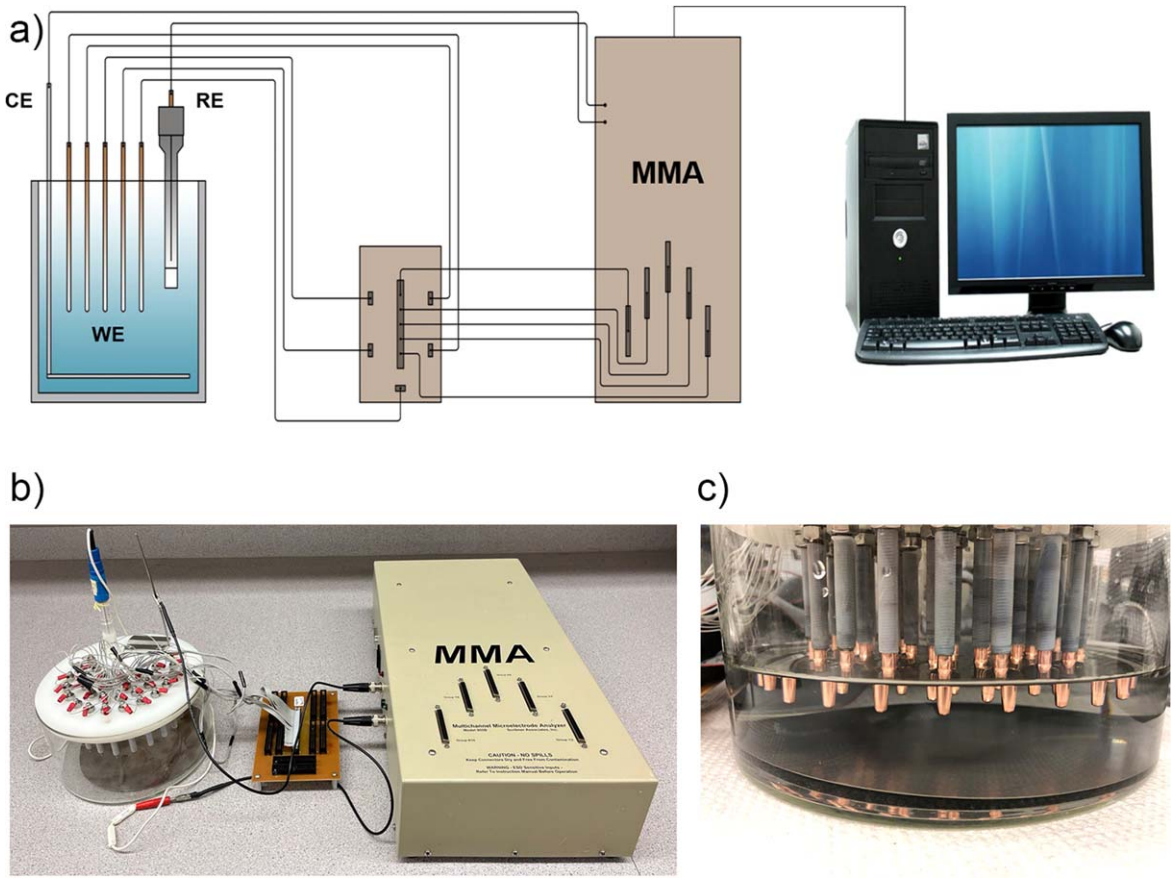

Figure 2. (a) Schematic of Multichannel Microelectrode Analyzer (MMA) connected to a multielectrode array (b) connection between multielectrode array and MMA through the interface and (c) inside view of the cell including working, and counter electrodes (reference electrode not visible).

reached 100 μA. A schematic of this procedure is shown in Fig. 3a, and the measured scans are plotted in f. We know from previous work[23] that, under all the conditions used in this work, this procedure results in the initiation of pitting corrosion on our Cu material. The E_b for each electrode was then determined from the intersection of the tangent to the current in the passive region with that of the rising current in the potential range after breakdown,[27,28] as demonstrated in Fig. 4b.

Our determinations of E_b were made using a linear extrapolation from the rising current (Fig. 4b), consistent with the Galvele IR drop theory,[29] but we also investigated the consequences of extrapolating from plots of log(i) and $\sqrt{i}$ vs E (in case of activation control or increasing active surface area withing hemispherical pits, respectively); however, we found that the extrapolation method had minimal influence on the E_b values determined, shifting them by only 2–10 mV.

Repassivation potential (E_{rp}) measurements.—The E_{rp} of Cu specimens undergoing pitting corrosion was measured under the same exposure conditions; however, to ensure that any observed

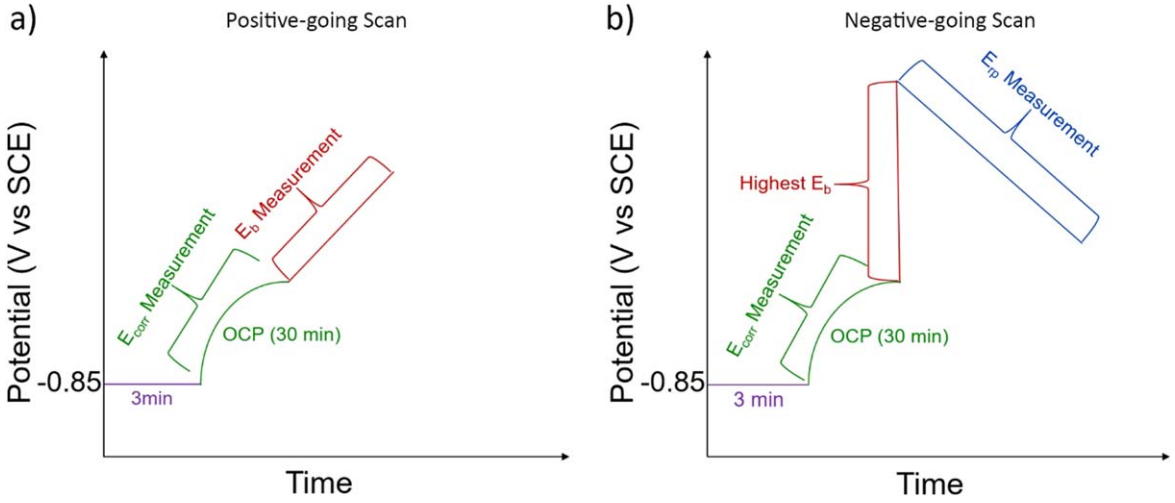

Figure 3. Schematic of electrochemical experiments with (a) positive-going scan for measurement of E_{corr} and E_b, and (b) negative-going scan for measurement of E_{rp}.

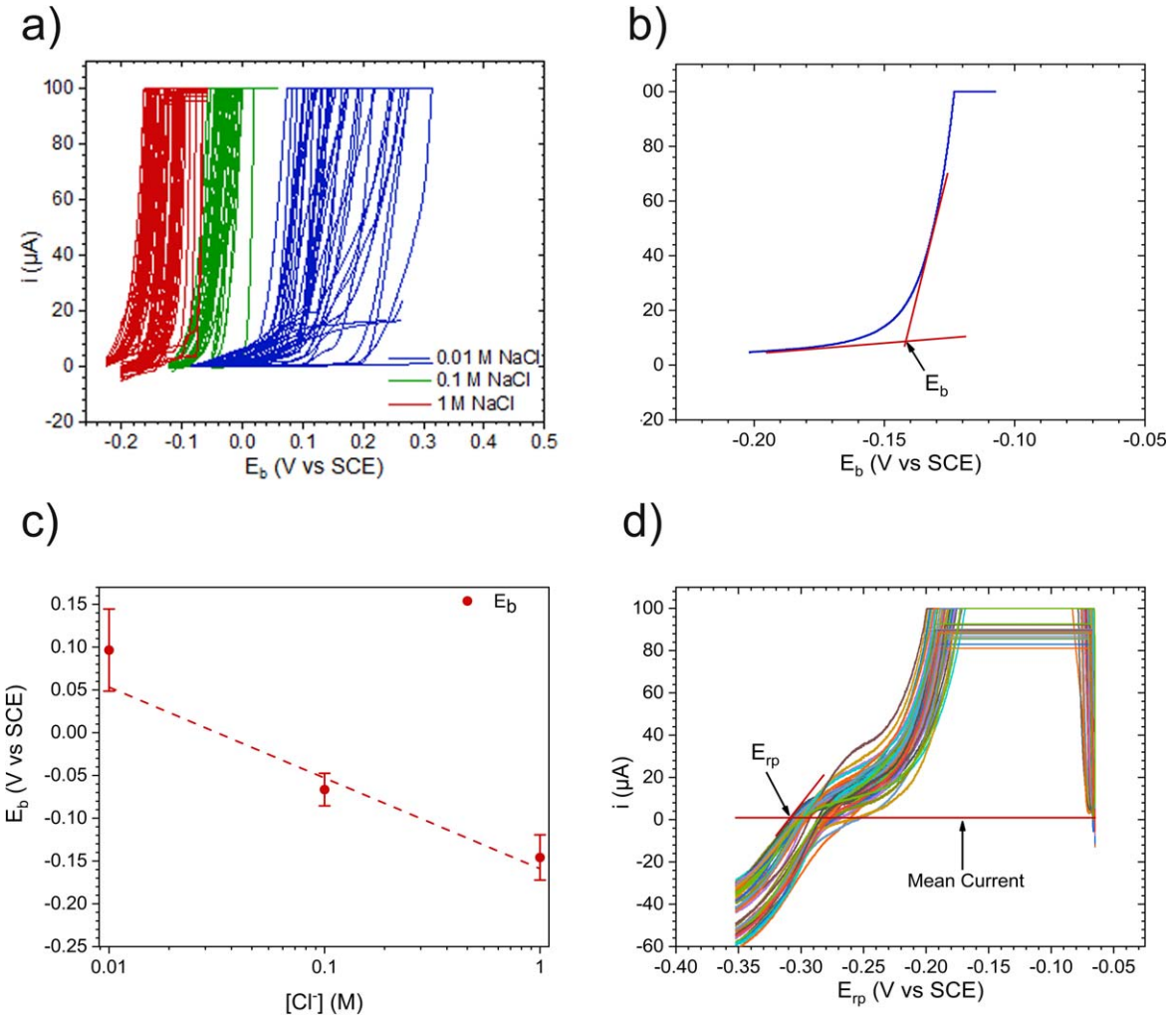

Figure 4. Determination of the breakdown potential of Cu from positive-going potential scans: (a) The many coloured curves represent the current traces recorded simultaneously on each of the 30 electrodes in the array exposed to room temperature NaCl solution at pH 11 at; (b) One of the scans with tangents drawn to demonstrate how the breakdown potential, E_b, was determined; (c) The ranges of E_b values measured at each chloride concentration, showing the changes in both the average potential and range of the potential distribution at each chloride concentration with the slope of −113 mV/deacade; and d) A series of negative-going "repassivation" scans that all started at E = −0.06 V vs SCE with a steep initial current rise as the electrodes immediately began to suffer pitting corrosion, followed by a flat region where the pitting current reached the maximum available from the potentiostat, followed by a declining current that allowed us to determine the repassivation potential E_{rp} at the point where the current declined to the mean value of the passive current density (red line) measured on positive-going scans under the same exposure conditions.

variation in E_{rp} values was not a result of differences introduced during the E_b measurement (as might be the case in traditional pitting scans that sweep the potential up to find E_b then back down again to find E_{rp}, thereby repassivating surfaces with differing degrees of pit initiation and growth), an identical preparation of all specimens was attempted, in terms of both surface preparation and the state of pit development prior to repassivation scans. To do this, Cu samples were ground as described in the sample preparation section to ensure that the surface condition of each electrode was the same before the pitting process. After the cathodic treatment and a 30-minute period of oxide growth at E_{corr}, all electrodes were simultaneously polarized in one step to a potential equivalent to the highest E_b value measured previously, such that pitting should initiate on all electrodes simultaneously. To determine the E_{rp} of each Cu electrode (Fig. 3b), a potentiodynamic scan in the negative direction was then conducted at a scan rate of 10 mV min^{-1} until the current of every electrode reached the mean passive current density previously measured during the scans to determine E_b (mean current in Fig. 5).

The E_{rp} on each electrode was taken as the potential at which the current on the negative-going scan reached the mean value of the original passive current observed in the positive-going scans.

Surface analysis.—After the breakdown experiment, samples were rinsed with Type I water, dried in a stream of Ar gas, and stored in an anaerobic chamber until they could undergo microscopic analysis. Scanning electron microscopy (SEM) was conducted to investigate the surface morphology and distribution of pits using a LEO 1540XB microscope (Zeiss Nano Technology System Division, Germany) located at Western Nanofabrication Facility.

Statistical treatment.—The multitude of E_{corr}, E_b, and E_{rp} measurements enabled by the multi-electrode array approach made it possible to perform statistical analyses of these parameters to estimate the likelihood that favourable conditions for pitting corrosion of Cu (either $E_{corr} > E_b$ or the more conservative $E_{corr} > E_{rp}$) could be achieved. The strategy employed was to determine a distribution function for each measured electrochemical parameter and integrate the area of overlap of the normalized distribution function of E_{corr} with that of either E_b or E_{rp} to yield a pitting probability value. The biggest obstacle to using this approach was that we do not possess the fundamental mechanistic information about the determinants of E_{corr}, E_b, and E_{rp} needed to allow the objective selection of one form of distribution function over another. Therefore, the strategy employed was to fit each set of data with a wide

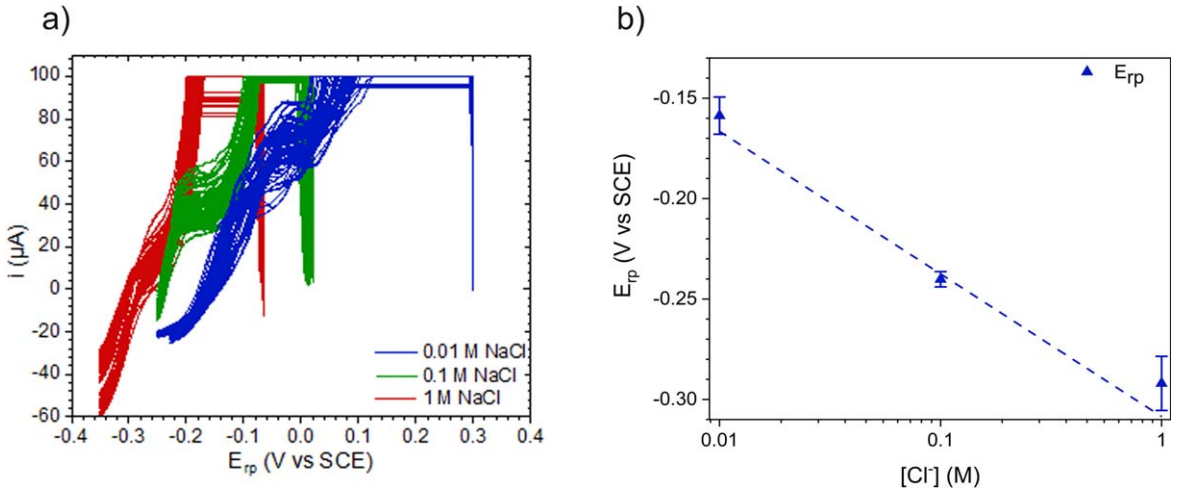

Figure 5. Repassivation potential of Cu electrodes in NaCl solution of pH 11 at room temperature: (a) Polarization scans of Cu in solutions containing 0.01, 0.1, and 1 M Cl^-; (b) Comparison of the mean and standard deviation of E_{rp} on Cu electrodes in solutions containing 0.01, 0.1, and 1 M Cl^- with the slope of −103 mV/deacade.

variety of known distribution functions and then calculate the predicted pitting probability for every combination of distribution function pairs (for those distribution functions for which a reasonable fit to the data could be achieved), to get an idea of the worst-case prediction of the pitting probability in each case.

Results and Discussion

Under neutral and acidic conditions Cl^- ions stabilize Cu(I) in the dissolved state as complex anions, $CuCl_x^{(x-1)-}$, with the value of x dependent on $[Cl^-]$.[24] Under these conditions, active corrosion would be expected, with the anodic dissolution process proceeding via the reaction sequence:

$$Cu(s) + Cl^-(\text{aq}) \rightarrow CuCl_{ads} + e^- \quad [1]$$

$$CuCl_{ads} + Cl^-(\text{aq}) \rightarrow CuCl_2^-{}_{ads} \quad [2]$$

$$CuCl_2^-{}_{ads} \rightarrow CuCl_2^-(aq) \quad [3]$$

where "ads" represents a surface-adsorbed state. The mass transport of $CuCl_x^{(x-1)-}$ from the Cu surface has been claimed to be rate-determining.[30,31]

As the pH increases from neutral to more alkaline values, the likelihood of oxide formation, and hence the possibility of pitting, increases, with the initial formation of oxide involving a competition for surface sites between Cl^- and OH^-,

$$CuCl_{ads} + OH^-(\text{aq}) \rightarrow Cu(OH)_{ads} + Cl^-(aq) \quad [4]$$

$$2Cu(OH)_{ads} \rightarrow Cu_2O(s) + H_2O \quad [5]$$

and the extent of oxide formation becoming dependent on the relative $[Cl^-]$ and $[OH^-]$ (i.e., pH).[24,32–36] Hydrolysis of dissolved $CuCl_x^{(x-1)-}$ can also result in Cu_2O growth:[31]

$$2CuCl_2^-(aq) + H_2O \rightarrow Cu_2O(s) + 2H^+(\text{aq}) + 4Cl^-(aq) \quad [6]$$

In the presence of a sufficient dissolved $[O_2]$, the homogeneous oxidation of $CuCl_x^{(x-1)-}$ can lead to the formation of Cu^{2+} and the deposition of Cu(II) solids, with atacamite being most likely in solutions containing a sufficiently high $[Cl^-]$,

$$12CuCl_2^-(\text{aq}) + 3O_2(\text{aq}) + 6\ \ H_2O \rightarrow 4Cu_2(OH)_3Cl(s)$$

$$+\ \ 4Cu^{2+}(\text{aq}) + 20Cl^-(aq) \quad [7]$$

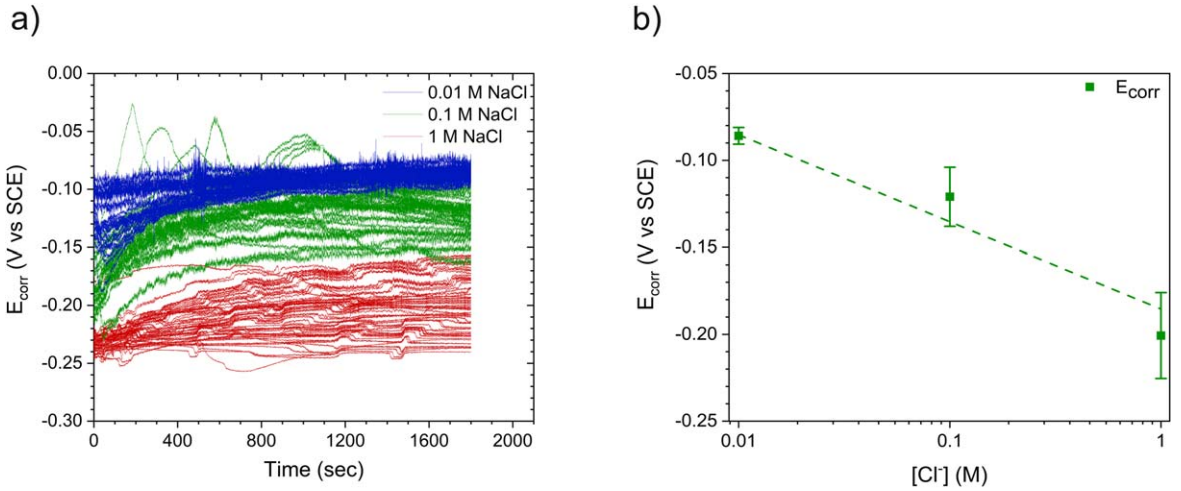

Figure 6. Corrosion potential of Cu electrodes in NaCl solution of pH 11 at room temperature: (a) E_{corr} values of Cu in solutions containing 0.01, 0.1, and 1 M Cl^-; and (b) Comparison of mean and standard deviation of E_{corr} values on Cu electrodes in solutions containing 0.01, 0.1, and 1 M Cl^- with the slope of −105 mV/deacade.

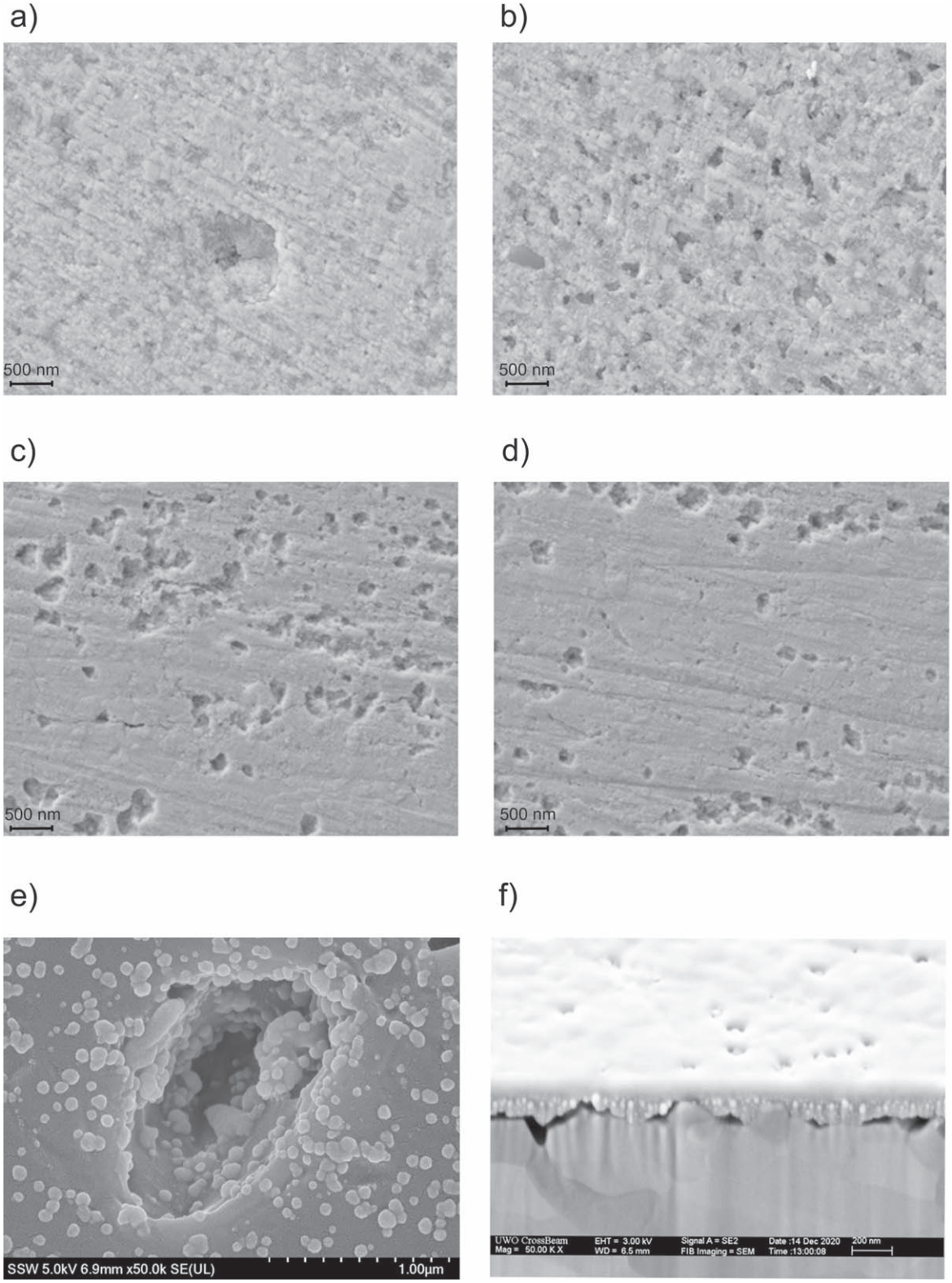

Figure 7. Scanning electron micrographs (SEM) of Cu surfaces after pitting experiments at room temperature in 1 M NaCl solution at pH 11: (a), (b) Surface morphology of Cu after exposure at the lowest E_b, (c), (d) Surface morphology of Cu after exposure at the highest E_b (e), (f) surface morphology and FIB-cut of Cu at potential close to the lowest E_b.

This leads to a duplex film comprising an inner layer of Cu_2O and an outer layer of deposited Cu(II) solids.[19–21,27,31,37] For low [Cl^-] and a sufficiently high pH, the deposited outer Cu(II) film becomes a poorly characterized mixture of CuO and $Cu(OH)_2$[20] with a thickness that increases with pH. For a sufficiently high pH ($\geqslant$12) the outer layer is dominantly $Cu(OH)_2$.[38]

What role these films play in establishing passivity remains only partially resolved, although it is clear that Cl^- exerts a significant

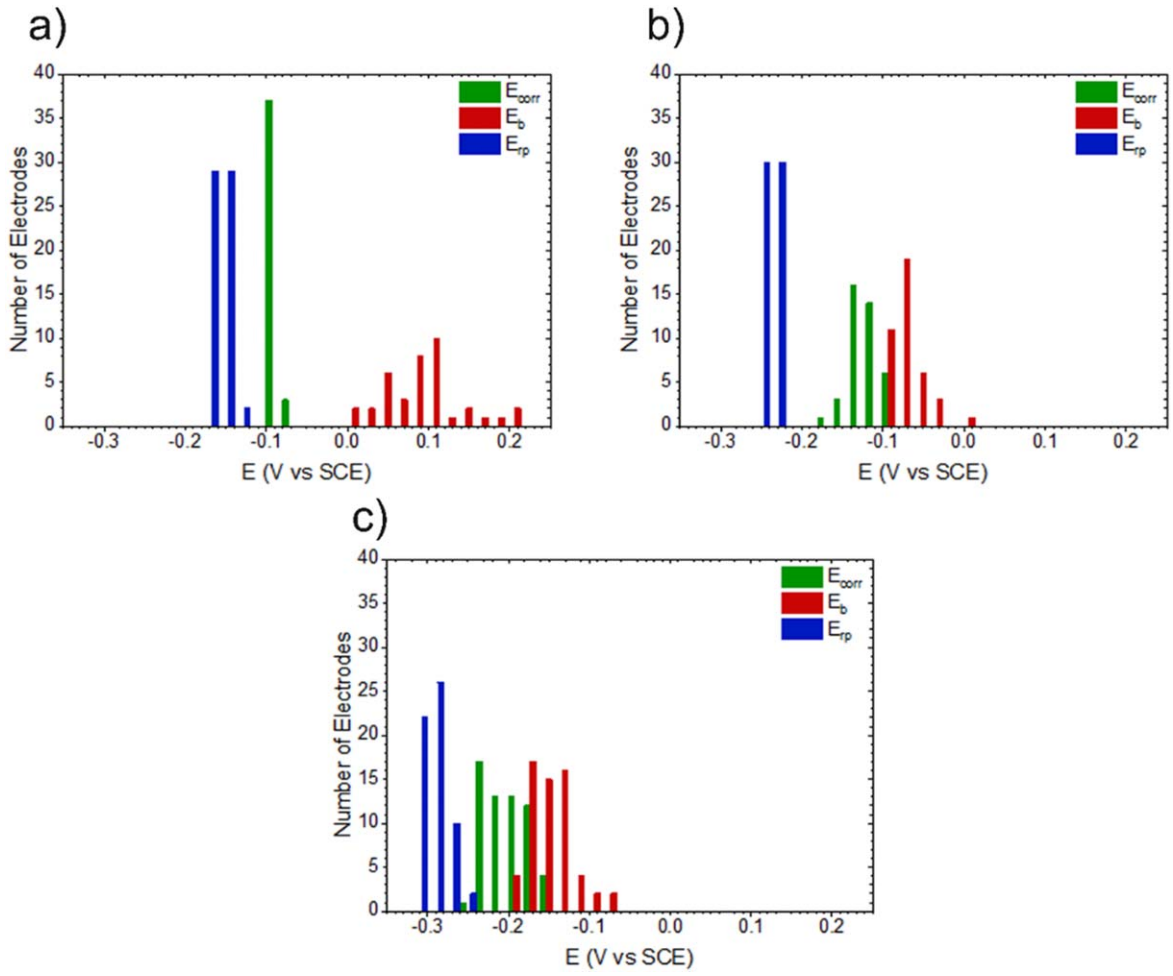

Figure 8. Histogram of E_{corr}, E_b, and E_{rp} values on Cu at room temperature in pH 11 solutions containing different chloride concentrations: (a) 0.01 M Cl^-; (b) 0.1 M Cl^-; and (c) 1 M Cl^-.

effect on the properties and stability of the films. The substitution of monovalent Cl^- ions for divalent O_2^- ions in the Cu_2O lattice creates defects, resulting in films that are less protective than those formed in the absence of Cl^-.[27,35,39,40] It has been claimed that islands of CuCl within an otherwise protective (passive) Cu_2O film can act as initiation sites for pitting[41] which would then be supported by O_2 reduction on the surrounding defective semiconducting Cu_2O. This suggests that depending on the [Cl^-], Cu_2O films formed in Cl^--containing solutions may be more susceptible to breakdown and pitting.[31,39]

E_{corr} measurements.—Figure 6a presents the E_{corr} of all electrodes in solutions with different chloride concentrations. In all solutions, E_{corr} increased with time, likely due to the formation of an oxide film[42,43] and the self-repair of defects within it over time. At higher [Cl^-], the average E_{corr} was observed at more negative values, while the range of E_{corr} values increased. The average E_{corr} and range are shown as a function of chloride concentration in Fig. 6b.

Both Cl^- and OH^- can adsorb on Cu surfaces at very low potentials,[31,35,39]

$$Cu(s) + OH^-(\text{aq}) \rightarrow CuOH_{ads} + e^- \quad [8]$$

$$Cu(s) + Cl^-(\text{aq}) \rightarrow CuCl_{ads} + e^- \quad [9]$$

with $CuOH_{ads}$ being a precursor to oxide formation:

$$2CuOH_{ads} \rightarrow Cu_2O(s) + H_2O \quad [10]$$

This competition offers a means for Cl^- to interfere with the oxide growth process, with Cl^- promoting dissolution, and OH^- mainly promoting film growth. At pH 11 the solubility of Cu_2O is beyond its minimum value, which occurs at ~pH 9.2.[31] Thus, film formation will be accompanied by dissolution,

$$CuOH_{ads} + OH^-(\text{aq}) \rightarrow Cu(OH)_2^-(aq) \quad [11]$$

$$CuCl_{ads} + Cl^-(\text{aq}) \rightarrow CuCl_2^-(aq) \quad [12]$$

with reaction 12 increasing in importance at higher [Cl^-]. In addition, as noted in the introduction, it is possible that $CuOH_{ads}$ and $CuCl_{ads}$ coexist on the surface, depending on the ratio of [OH]/[Cl^-]. Thus, the lower E_{corr} at higher [Cl^-] can be attributed to a combination of a greater influence of Cl^- on passive film properties, accompanied by enhanced Cu(I) dissolution as $CuCl_2^-$.

E_b measurements.—The pitting scans are shown in Fig. 4a and average E_b and range are given as a function of chloride concentration in Fig. 4c. Scanning electron microscopy (SEM) was used to verify that pitting occurred on the Cu surfaces and to investigate the surface morphology of electrodes after pitting breakdown scans in 1 M Cl^- solution (Fig. 7). The plan views of the electrodes with the highest and lowest E_b values show surfaces extensively covered with small pits. A focused ion beam cross section through a small pit (Fig. 7f) shows an elongated area of damage located between two grains.

The E_b values were more negative at higher chloride concentrations, in keeping with the general observations of others.[18,24,28,31,40,44–47]

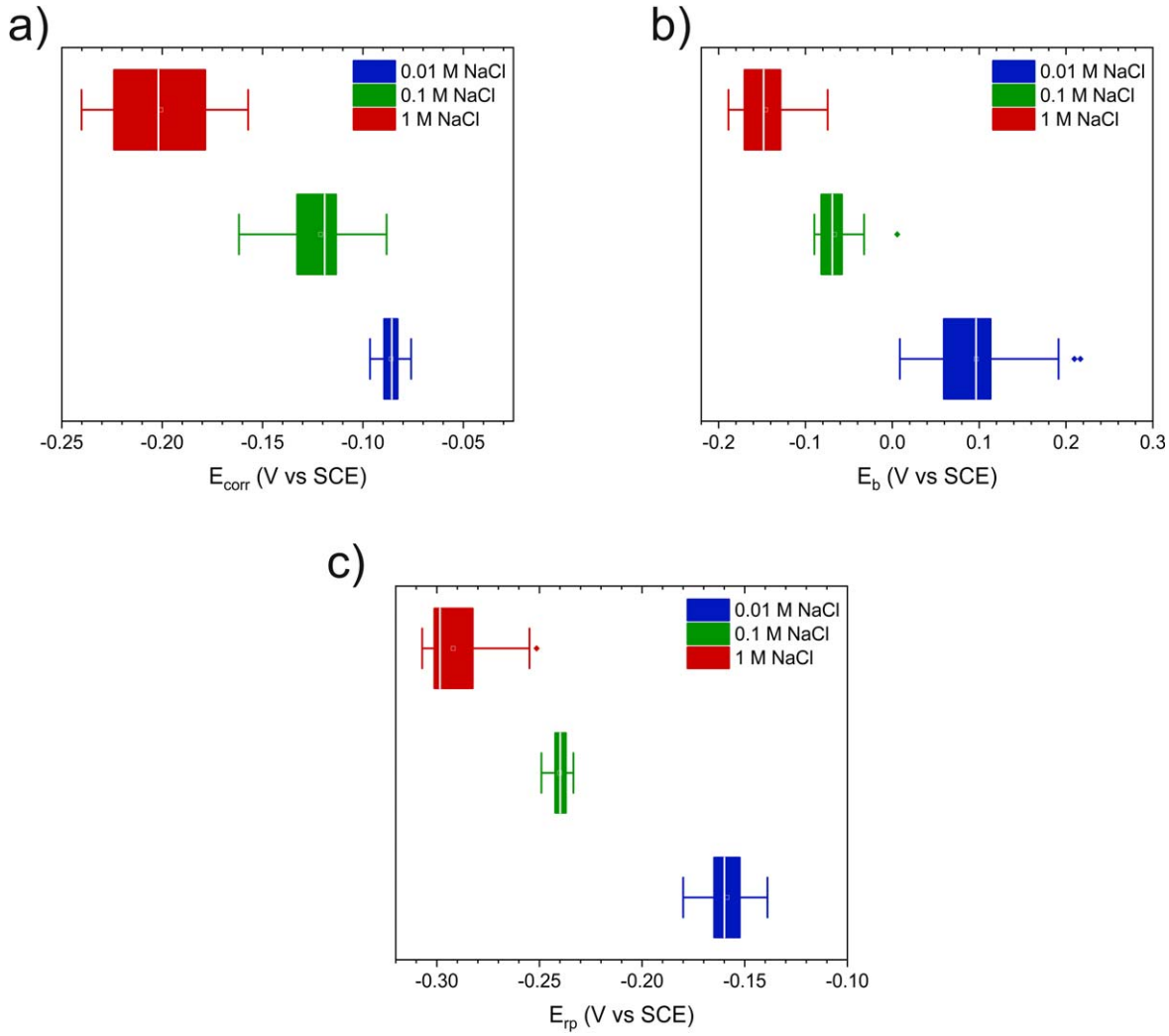

Figure 9. Box plot of corrosion parameters measured on Cu in NaCl solution of pH 11 at room temperature with different [Cl^-]: (a) E_{corr}, (b) E_b, and (c) E_{rp}.

Starosvetsky et al.[46] observed local copper activation (pitting) in low-chloride solutions, while activation extended rapidly over the whole electrode surface in high-chloride solutions; however, other researchers demonstrated that decreasing the chloride concentration improved the density and decreased the porosity of the passive film, which resulted in a higher E_b.

The relationship between E_b and log [Cl^-] has previously been proposed to be linear,[48,49] with a slope depending on the nature of the passive film, number of electrons transferred, and other features, and our results were in keeping with those expectations (Fig. 4c). A semi-logarithmic relation between the E_b and [Cl^-], with the form,

$$E_b = A - B \quad log\,[Cl^-] \qquad [13]$$

where A and B are constants, has also been observed for other systems, including iron, nickel, and stainless steel.[29] However, Galvele[29] proposed that the pitting potential depends on the potential drop (IR) in the pit nucleus, so the IR drop should be subtracted from the measured E_b to get the true E_b. Figure 4c shows that the E_b vs log [Cl^-] plot has a slope of −113 mV/decade, suggesting a one-electron reaction, leading to a surface covered with Cu(I) oxide.

E_{rp} measurements.—Figure 5a shows that E_{rp} was found at more negative potentials in solutions with higher [Cl^-], which is in good agreement with the literature.[20] The average E_{rp} values and range are shown as a function of chloride concentration in Fig. 5b. These measurements suggest that pit propagation would be possible in all the chloride-containing solutions used, since the distributions of E_{rp} values were located at potentials more negative than the potential range over which E_{corr} was distributed (Fig. 8).[19,21] The distributions of E_{rp} values for Cu in solutions of different [Cl^-] were narrow compared to those of E_{corr} and, especially, E_b (Fig. 9). The magnitudes of the slopes of $dE_{corr}/dlog[Cl^-]$, $dE_b/dlog[Cl^-]$, and $dE_{rp}/dlog[Cl^-]$ were similar (Figs. 4c, 5b, 6b) at just over −100 mV/decade of [Cl^-]. Cong[20] reported a strong dependency of E_{corr} and E_b, and weak dependency of E_{rp}, on the [Cl^-]. By contrast, our results indicate strong dependency for E_b and similar dependencies for E_{corr} and E_{rp}, as reported for stainless steel.[8,50]

Statistical analysis.—Box plots of E_{corr}, E_b, and E_{rp} are shown in Fig. 9. The interquartile range (IQR) of E_{corr} for different chloride concentrations indicated a wider dispersion in 1 M Cl^- solution than in 0.01 and 0.1 M Cl^- solutions, and no outliers were observed under any of the conditions tested, which indicated a light tail distribution under all conditions.

Increasing the chloride concentration shifted the E_{corr} in the negative direction. The dispersion of E_b decreased with increasing [Cl^-] up to 0.1 M; however, a further increase in [Cl^-] resulted in a larger IQR. Outliers were observed in the data for 0.01 and 0.1 M Cl^- solutions, which indicated the possibility of a heavy tail distribution (right-skewed) under those conditions; however, no outliers were observed in the data collected from experiments conducted in 1 M Cl^- solutions. The IQR of E_{rp} decreased with increasing [Cl^-] from 0.01 to 0.1 M, while a further increase in

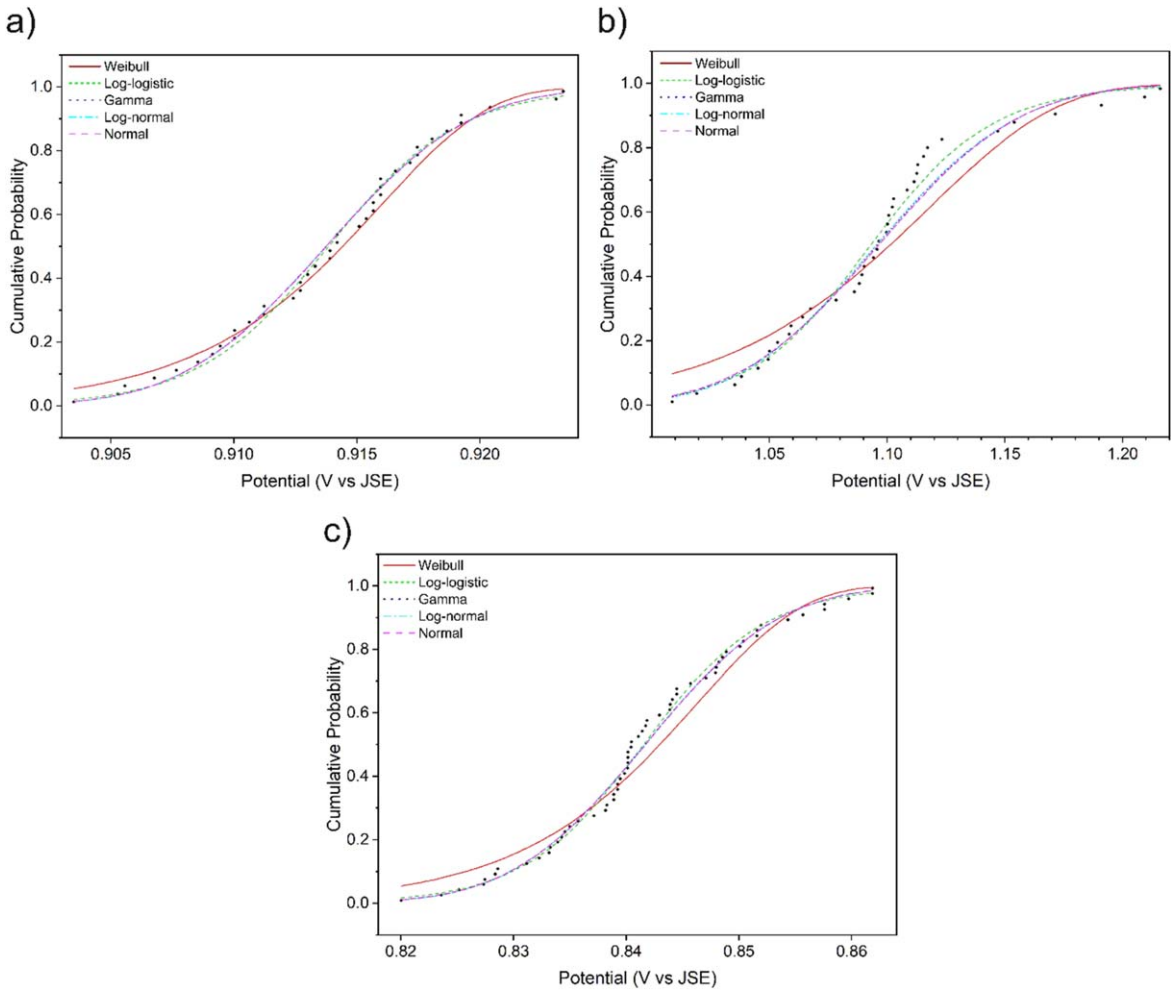

Figure 10. Cumulative distribution function (CDF) of experimental data and simulated models for Cu in 0.01 M NaCl solution of pH 11 at room temperature: (a) E_{corr}; (b) E_b; (c) E_{rp}.

$[Cl^-]$ to 1 M contributed to a larger IQR, with the presence of an outlier, changing the shape of the distribution to a right-skewed distribution. This heavy tail might increase the probability of repassivation, as it is located on the right side of the E_{rp} distribution, which might result in a greater chance of $E_{corr} < E_{rp,}$ which is the necessary condition for repassivation.

Since we have no theoretical basis upon which to base a prediction of the distributions of the values of the measured corrosion parameters, the collections of measured E_{corr}, E_b, and E_{rp}, values were fitted with a variety of different distribution functions to determine whether any of these functions provided reasonable representations of the measured data. Some gave reasonable fits whereas others differed significantly from the measured data. In the end, five distribution functions were selected for use in the analysis, based on the quality of fit with a confidence level of 90%. One key mathematical requirement of the statistical models used is that all of the input parameters be positive-valued. To achieve this, we shifted all measured potentials by an arbitrary 1 V in the positive direction (indicated by the artificial potential scale designated "JSE," where E (V vs JSE) = E (V vs SCE + 1 V)). Such a translation of potential values enables the statistical analysis to be applied without affecting its outcome, because it ensures that all potential values are positive in sign without changing their positions relative to each other.

The cumulative distribution functions (CDF) and probability density functions (PDF) of E_{corr}, E_b, and E_{rp} for the three chloride-containing solutions used are shown in Fig. 10 through Fig. 14. The PDF plots indicate the probability of pitting based on the overlap between the distribution curves of E_{corr} and E_b (Fig. 13). Since we have no theoretical basis for choosing between the distribution functions that fit reasonably well, we calculated the pitting probability for every combination of distribution functions representing E_{corr} and E_b values. Table I shows the pitting probabilities calculated from the overlap of each possible pair of distribution functions. To make a conservative prediction of the pitting probability, we take the highest probability value determined by this method for each data set. Under these conditions, a greater probability of Cu pitting was observed in 1 M Cl^- solutions than in 0.01 and 0.1 M Cl^- solutions. Previous publications showed the same trend of pitting probability of copper;[19,21,44] however, King[31] determined a lower probability of pitting in solutions with higher chloride concentrations. He determined a very low probability of pitting in an alkaline solution containing a high chloride concentration, since $E_{corr} \ll E_b$. It is important to note that statistical analysis should be considered based on an acceptable number of data, while King's analysis was based on only a few data points, which decreased the accuracy of the statistical analysis compared to our analysis, consisting of more than 120 data points.

The overlap between the PDFs of E_{corr} and E_{rp} in f indicate the repassivation probability of Cu, since the PDF of E_{rp} is located to the left side of E_{corr} in this case. A lower probability of repassivation was observed in lower $[Cl^-]$ solutions than in higher $[Cl^-]$ solutions, possibly due to the concentration of dissolved copper species in the bottom of pits in solutions with high chloride concentration, which triggered the repassivation of Cu (Table II).

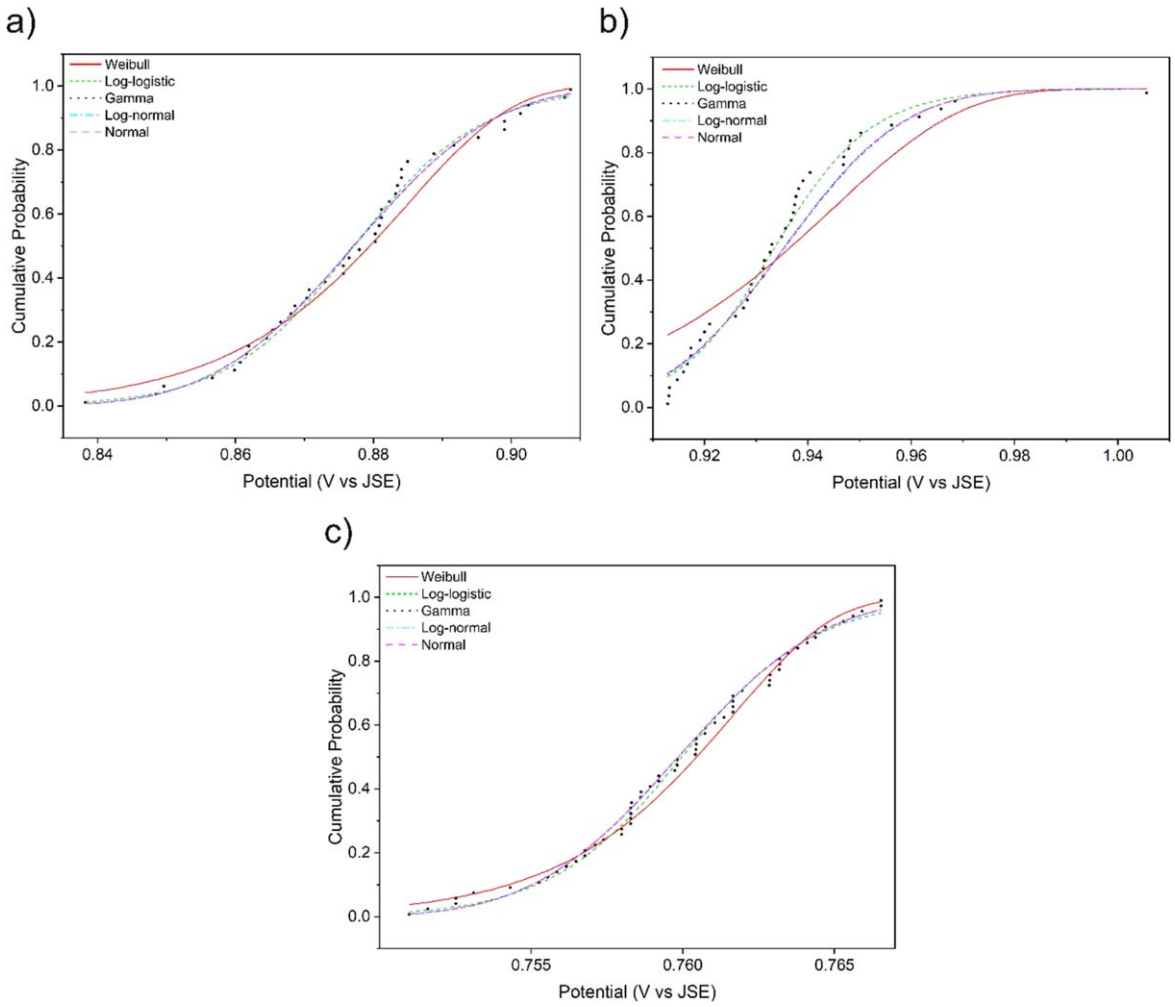

Figure 11. Cumulative distribution function (CDF) of experimental data and simulated models for Cu in 0.1 M NaCl solution of pH 11 at room temperature: (a) E_{corr}; (b) E_b; (c) E_{rp}.

Table I. Pitting probability (%) of Cu in different chloride-containing solutions (a) 0.01 M Cl^- (b) 0.1 M Cl^- (c) 1 M Cl^- based on different distribution functions.

		Corrosion Potential (E_{corr})				
Breakdown Potential (E_b)	Distribution	Log-Logistic	Gamma	Log-Normal	Normal	Weibull
a)						
	Log-Logistic	5.69×10^{-3}	1.52×10^{-11}	3.06×10^{-10}	1.04×10^{-10}	9.06×10^{-2}
	Gamma	5.06×10^{-3}	1.52×10^{-11}	3.06×10^{-10}	1.04×10^{-10}	7.97×10^{-4}
	Log-Normal	4.93×10^{-3}	1.52×10^{-11}	3.06×10^{-10}	1.04×10^{-10}	3.74×10^{-4}
	Normal	5.69×10^{-3}	1.52×10^{-11}	3.06×10^{-10}	1.04×10^{-10}	3.08×10^{-3}
	Weibull	1	1	1	1	1
b)						
	Log-Logistic	12	12	12	12	10
	Gamma	13	12	12	12	10
	Log-Normal	12	12	12	12	1
	Normal	13	13	13	13	11
	Weibull	25	24	24	24	23
c)						
	Log-Logistic	28	28	28	28	29
	Gamma	28	28	28	28	29
	Log-Normal	28	28	28	28	29
	Normal	28	28	28	28	29
	Weibull	34	34	34	34	34

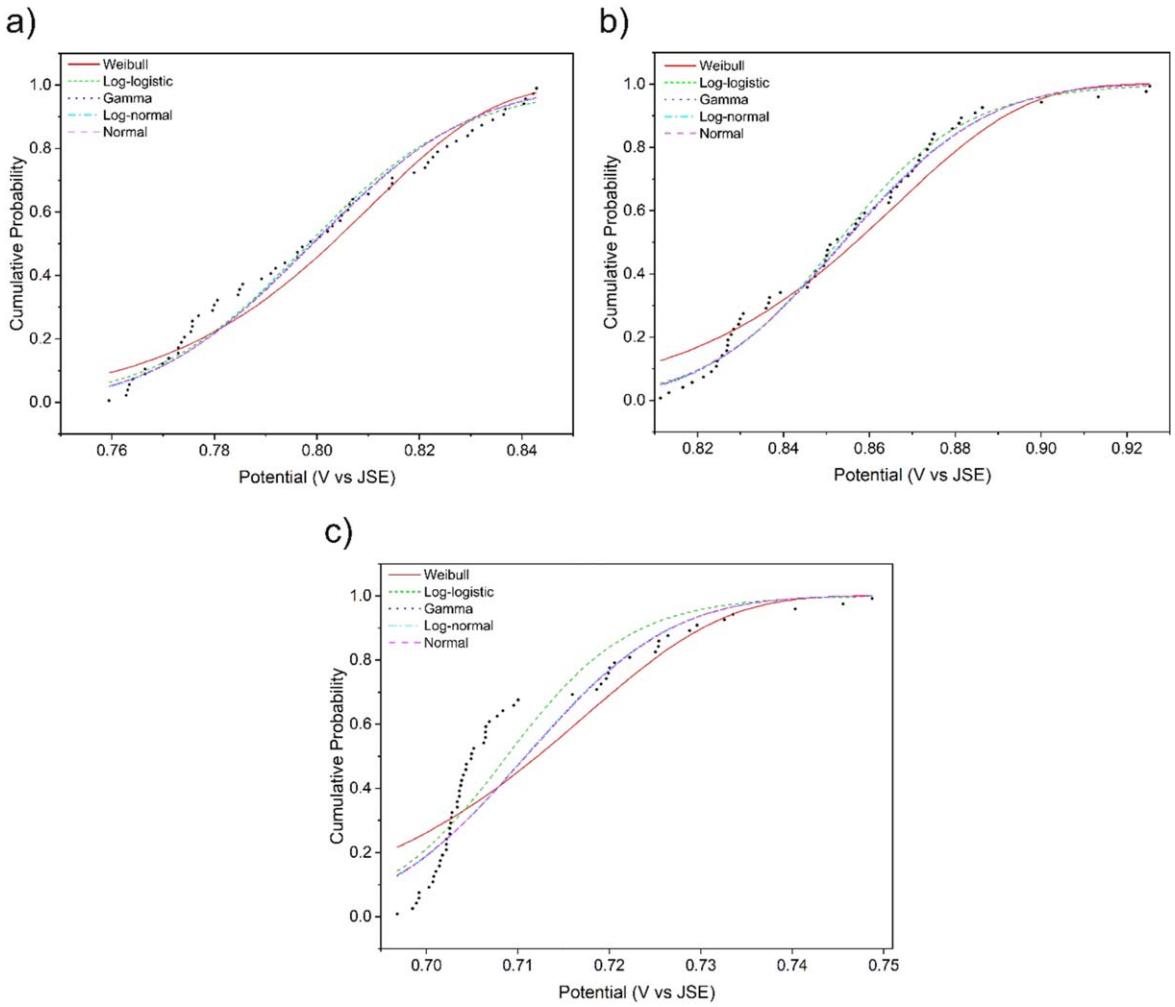

Figure 12. Cumulative distribution function (CDF) of experimental data and simulated models for Cu in 1 M NaCl solution of pH 11 at room temperature: (a) E_{corr}; (b) E_b; (c) E_{rp}.

Table II. Repassivation probability (%) of Cu in different chloride-containing solutions (a) 0.01 M Cl^-, (b) 0.1 M Cl^-, (c) 1 M Cl^-, based on different distribution functions.

		Corrosion Potential (E_{corr})				
Repassivation Potential (E_{rp})	Distribution	Log-Logistic	Gamma	Log-Normal	Normal	Weibull
a)						
	Log-Logistic	8.32×10^{-4}	2.12×10^{-10}	3.06×10^{-10}	1.04×10^{-10}	8.93×10^{-2}
	Gamma	8.29×10^{-4}	5.20×10^{-13}	1.74×10^{-14}	8.68×10^{-14}	2.31×10^{-4}
	Log-Normal	8.29×10^{-4}	5.20×10^{-13}	1.74×10^{-14}	8.68×10^{-14}	2.83×10^{-4}
	Normal	8.29×10^{-4}	5.20×10^{-13}	1.74×10^{-14}	8.68×10^{-14}	1.67×10^{-3}
	Weibull	9.81×10^{-10}	1.59×10^{-47}	1.59×10^{-47}	1.59×10^{-47}	2.32×10^{-5}
b)						
	Log-Logistic	1.57×10^{-4}	5.30×10^{-8}	2.16×10^{-8}	2.89×10^{-7}	8.56×10^{-2}
	Gamma	1.57×10^{-4}	5.30×10^{-8}	2.16×10^{-8}	2.89×10^{-7}	3.93×10^{-3}
	Log-Normal	1.57×10^{-4}	5.30×10^{-8}	2.16×10^{-8}	2.89×10^{-7}	3.63×10^{-3}
	Normal	1.57×10^{-4}	5.30×10^{-8}	2.16×10^{-8}	2.89×10^{-7}	4.62×10^{-3}
	Weibull	6.92×10^{-6}	1.44×10^{-21}	4.24×10^{-23}	8.62×10^{-19}	1.88×10^{-3}
c)						
	Log-Logistic	3	2	2	2	5
	Gamma	2	1	1	2	5
	Log-Normal	2	1	1	2	5
	Normal	2	4.75×10^{-3}	4.75×10^{-3}	4.75×10^{-3}	5
	Weibull	2	1	1	2	5

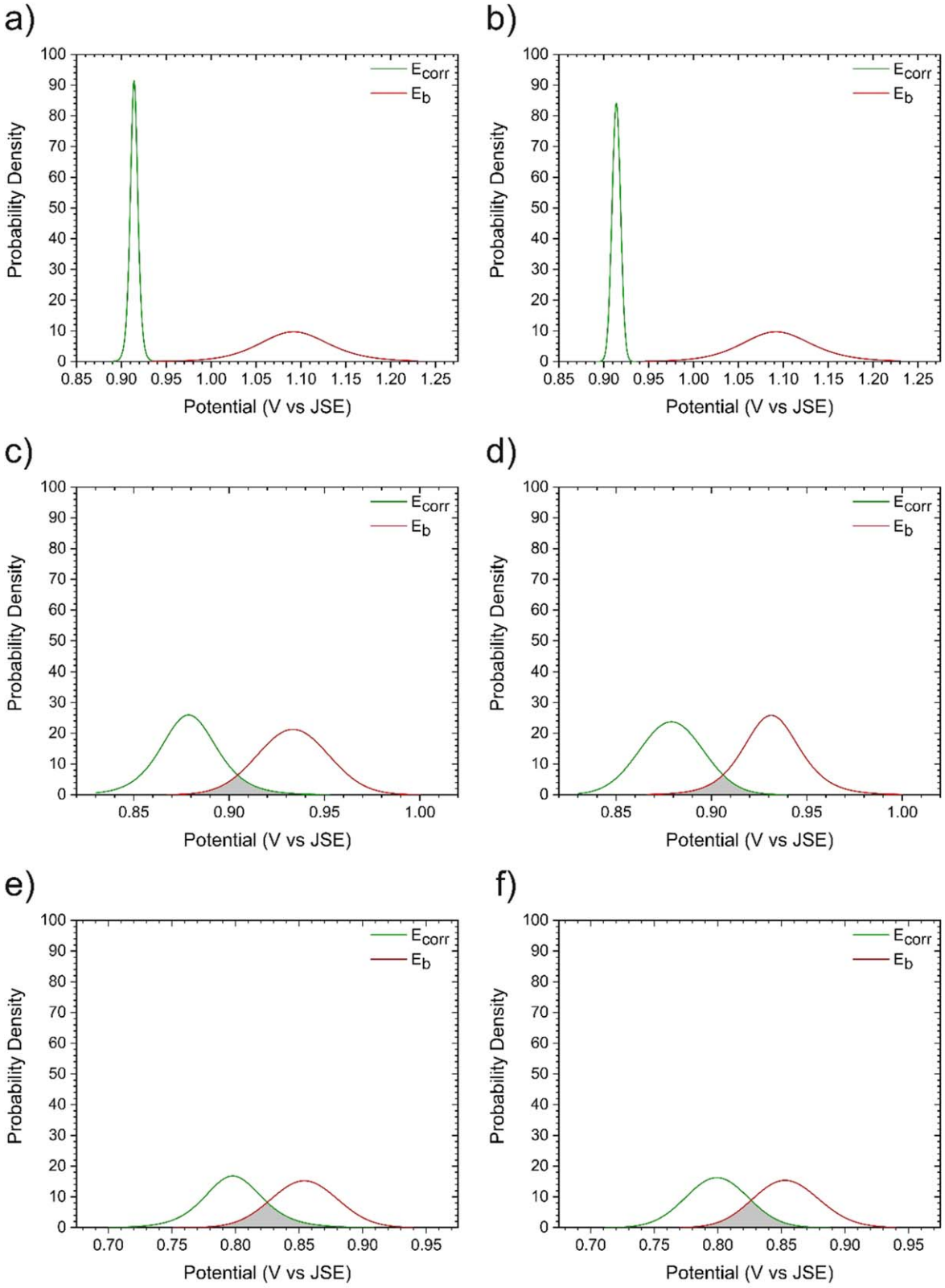

Figure 13. Probability distribution curves of E_{corr} and E_b on Cu in NaCl solution of pH 11 at room temperature: (a), (b) Maximum and minimum overlaps between E_{corr} and E_b in 0.01 M Cl^- solution, respectively; (c), (d) Maximum and minimum overlaps between E_{corr} and E_b in 0.1 M Cl^- solution, respectively; (e), (f) Maximum and minimum overlaps between E_{corr} and E_b in 1 M Cl^- solution, respectively.

Conclusions

The probability of pitting corrosion of copper in pH 11 solution with different chloride concentrations has been studied using a multielectrode array to generate large numbers of data that enable the application of statistical analyses of the processes involved. The corrosion potential decreased with increasing chloride concentration and the dispersion of E_{corr} data increased with [Cl^-]; however,

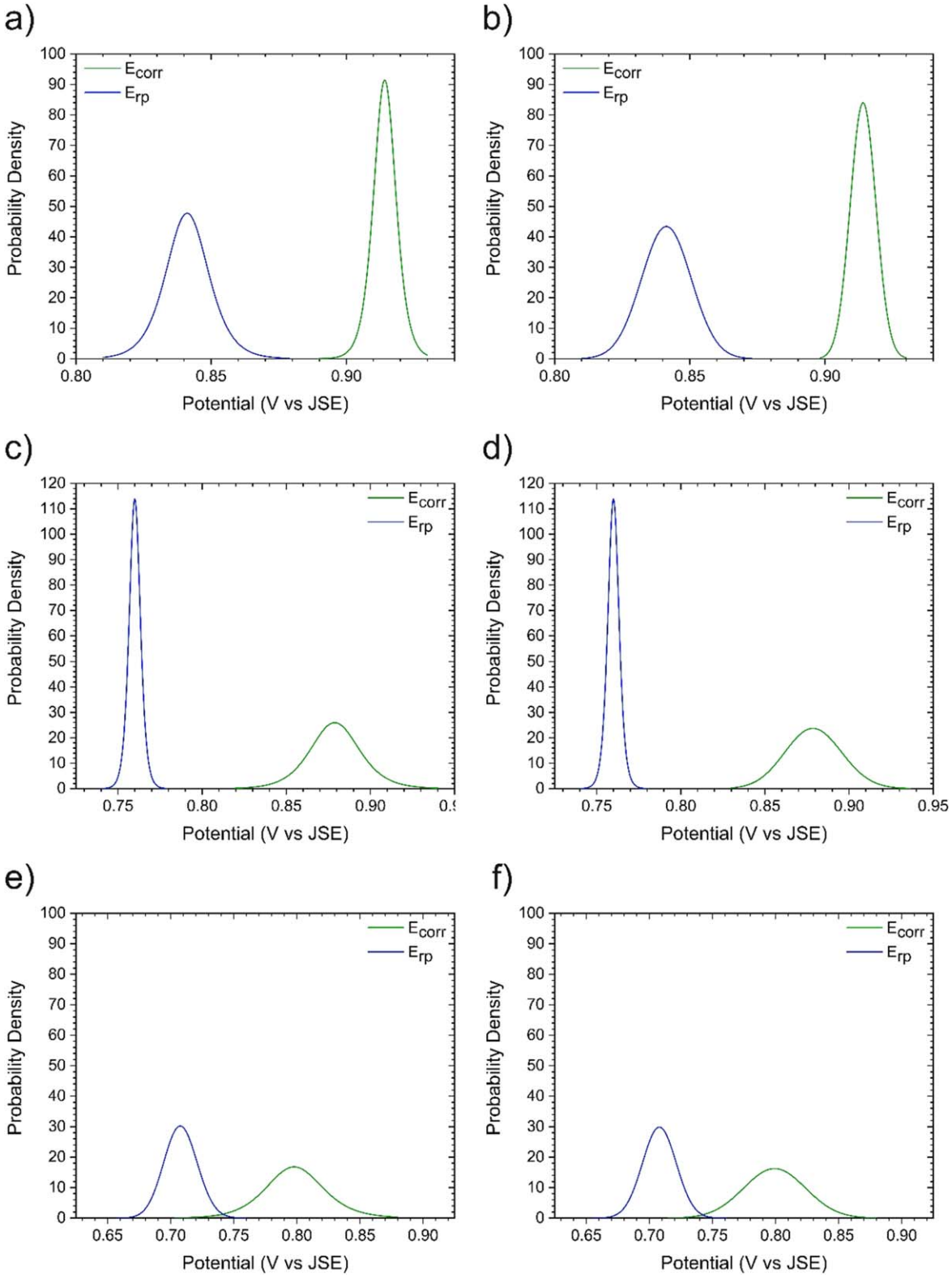

Figure 14. Probability distribution curves of E_{corr} and E_{rp} on Cu in NaCl solution of pH 11 at room temperature: (a), (b) Maximum and minimum overlaps between E_{corr} and E_{rp} in 0.01 M Cl^-, respectively; (c), (d) Maximum and minimum overlaps between E_{corr} and E_{rp} in 0.1 M Cl^-, respectively; (e), (f) Maximum and minimum overlaps between E_{corr} and E_{rp} in 1 M Cl^-, respectively.

dispersion of E_b and E_{rp} decreased with increasing [Cl^-] up to 0.1 M and then increased with further increase of [Cl^-] to 1 M. Distributions in the values of E_b and E_{rp} could be due to the stochastic nature of passive film breakdown and reformation. Investigations of the pitting probability show a greater overlap between the PDFs of E_{corr} and E_b, and of E_{corr} and E_{rp}, respectively, in solutions with higher chloride concentrations, indicating a higher probability of both pit initiation and repassivation. The further development of this approach will involve investigations of scan rate, hold time, pH, dissolved anions, temperature, dissolved oxygen concentration and other likely influential parameters.

Acknowledgments

This research was jointly funded by the Nuclear Waste Management Organization (NWMO), Toronto and the Natural Sciences and Engineering Research Council of Canada (NSERC) under a Collaborative Research and Development grant (CRDPJ 507465-16). Assistance provided by personnel at Engineering Machine Shop and Western Nanofabrication Facility is gratefully acknowledged.

ORCID

Sina Matin https://orcid.org/0000-0002-5339-9313
James J. Noël https://orcid.org/0000-0003-3467-4778

References

1. G. R. Engelhardt and D. D. Macdonald, *J. Electrochem. Soc.*, **167** 013540 (2020).
2. Y. Zhou, A. Xu, F. Mao, J. Yu, D. Kong, C. Dong, and D. D. Macdonald, *Electrochim. Acta*, **320**, 1 (2019).
3. D. D. Macdonald and M. Urquidi-Macdonald, *Electrochim. Acta*, **31**, 1079 (1986).
4. T. Haruna and D. D. Macdonald, *J. Electrochem. Soc.*, **144**, 1574 (1997).
5. G. Engelhardt and D. D. Macdonald, *Corros. Sci.*, **46**, 2755 (2004).
6. P. M. Aziz, *Corrosion*, **12**, 35 (1956).
7. G. G. Eldredge, *Corrosion*, **13**, 67 (1957).
8. T. Shibata, *Corrosion*, **52**, 813 (1996).
9. V. F. Lucey, *Br. Corros. J.*, **2**, 175 (1967).
10. H. M. Shalaby, F. M. Al-Kharafi, and V. K. Gouda, *Corrosion Journal*, **45**, 536 (1989).
11. N. J. Laycock, M. H. Moayed, and R. C. Newman, *Journal of Electrochemical Society*, **145**, 2622 (1998).
12. R. Qvarfort, *Corros. Sci.*, **29**, 987 (1989).
13. V. M. Salinas-Bravo and R. C. Newman, *Corros. Sci.*, **36**, 67 (1994).
14. T. Li, J. R. Scully, and G. S. Frankel, *J. Electrochem. Soc.*, **165**, C484 (2018).
15. D. E. Williams, J. Stewart, and P. Balkwill, *Corros. Sci.*, **36**, 1213 (1994).
16. A. M. Riley, D. B. Wells, and D. E. Williams, *Corros. Sci.*, **32**, 1307 (1991).
17. D. E. Williams, C. Westcott, and M. Fleischmann, *Electrochemical Society*, **132**, 1796 (1985).
18. M. R. G. D. Chialvo, R. C. Salvarezza, D. V. Moll, and A. J. Arvia, *Electrochim. Acta*, **30**, 1501 (1985).
19. H. Cong and J. R. Scully, *J. Electrochem. Soc.*, **157**, 36 (2010).
20. H. Cong, H. T. Michels, and J. R. Scully, *Journal of Electrochemical Society*, **156**, 16 (2009).
21. H. Cong and J. R. Scully, *J. Electrochem. Soc.*, **157**, 200 (2010).
22. H. Ha, C. Taxén, H. Cong, and J. R. Scully, *J. Electrochem. Soc.*, **159**, C59 (2011).
23. Z. Qin, R. Daljeet, M. Ai, N. Farhangi, J. J. Noël, S. Ramamurthy, D. Shoesmith, F. King, and P. Keech, *Corrosion Engineering, Science and Technology*, **52**, 45 (2017).
24. A. E. Warraky, H. A. E. Shayeb, and E. M. Sherif, *Anti-Corrosion Methods and Materials*, **51**, 25 (2004).
25. F. King, D. S. Hall, and P. G. Keech, *Corrosion Engineering, Science and Technology*, **52**, 25 (2017).
26. D. S. Hall, M. Behazin, W. J. Binns, and P. G. Keech, *Prog. Mater Sci.*, **118**, 100766 (2021).
27. G. Mankowski, J. P. Duthil, and A. Giusti, *Corros. Sci.*, **39**, 27 (1997).
28. F. Mao, C. Dong, S. Sharifi-Asl, P. Lu, and D. D. Macdonald, *Electrochim. Acta*, **144**, 391 (2014).
29. J. R. Galvele, *Journal of Electrochemical Society*, **123**, 464 (1976).
30. F. King, *Critical review of the literature on the corrosion of copper by water TR-10-69*, Swedish Nuclear Fuel and Waste Management Co (2010), https://inis.iaea.org/collection/NCLCollectionStore/_Public/42/093/42093282.pdf.
31. F. King, *Corrosion of copper in alkaline chloride environment TR-02-25*, Swedish Nuclear Fuel and Waste Management Co (2002), https://www.skb.com/publication/19607/TR-02-25.pdf.
32. H. P. Lee and K. Nobe, *Journal of Electrochemical Society*, **133**, 2035 (1986).
33. C. Deslouis, B. Tribollet, G Mengoli, and M. M. Musiani, *Journal of Applied Electrochemistry*, **18**, 374 (1988).
34. B. Millet, C. Fiaud, C. Hinnen, and E. M. M. Sutter, *Corros. Sci.*, **37**, 1903 (1995).
35. F. King, L. Ahonen, C. Taxen, U. Vuorinen, and L. Werme, *Copper corrosion under expected conditions in a deep geologic repository*, Swedish Nuclear Fuel and Waste Management Co (2001), https://www.skb.com/publication/18994/TR-01-23.pdf.
36. G. Kear, B. D. Barker, and F. C. Walsh, *Corros. Sci.*, **46**, 109 (2004).
37. H. H. Strehblow and B. Titze, *Electrochim. Acta*, **25**, 839 (1980).
38. D. W. Shoesmith, T. E. Rummery, D. Owen, and W. Lee, *Electrochim. Acta*, **22**, 1403 (1977).
39. F. King, C. Lilja, K. Pedersen, P. Pitkänen, and M. Vähänen, *An update of the state-of-the-art report on the corrosion of copper under expected conditions in a deep geologic repository*, Swedish Nuclear Fuel and Waste Management Co (2010), https://www.skb.com/publication/18994/TR-01-23.pdf.
40. H. Ha, C. Taxen, K. Williams, and J. Scully, *Electrochim. Acta*, **56**, 6165 (2011).
41. E. Mattson, *Br. Corros. J.*, **15**, 6 (1980).
42. M. A. Abdulhay and A. A. Al-Suhybani, *Materials Science and Engineering Technology*, **23**, 407 (1992).
43. T. Standish, J. Chen, R. Jacklin, P. Jakupi, S. Ramamurthy, D. Zagidulin, P. Keech, and D. Shoesmith, *Electrochim. Acta*, **211**, 331 (2016).
44. F. Arjmand and A. Adriaens, *Materials*, **5**, 2439 (2012).
45. M. Ochoa, M. A. Rodríguez, and S. B. Farina, *Procedia Materials Science*, **9**, 460 (2015).
46. D. Starosvetsky, O. Khaselev, M. Auinat, and Y. Ein-Eli, *Electrochim. Acta*, **51**, 5660 (2006).
47. A. Nishikata, M. Itagaki, T. Tsuru, and S. Haruyama, *Corros. Sci.*, **31**, 287 (1990).
48. A. G. G. Allah, M. M. Abou-Romia, W. A. Badawy, and H. H. Rehan, *Mater. Corros.*, **42**, 584 (1991).
49. G. Bianchi, G. Fiori, P. Longhi, and F. Mazza, *Corrosion*, **34**, 396 (1978).
50. T. Shibata and T. Takeyama, *Corrosion Journal*, **33**, 243 (1977).